Radiation-Induced Synthesis and Cryo-TEM Characterization of Silver Nanoshells on Linoleate Spherical Micelles

ARTICLE *in* LANGMUIR · OCTOBER 2007

Impact Factor: 4.46 · DOI: 10.1021/la701366f · Source: PubMed

Radiation-Induced Synthesis and Cryo-TEM Characterization of Silver Nanoshells on Linoleate Spherical Micelles

J. Attia,*,† S. Rémita,†,‡ S. Jonic,§ E. Lacaze,† M.-C. Fauré,† E. Larquet,§ and M. Goldmann†

Institut des Nanosciences de Paris (Université Pierre et Marie Curie, INSP-UMR7588, Paris, F-75005 France, CNRS, INSP-UMR7588, Paris, F-75005 France; Université Paris Diderot), Campus Boucicaut, 140 rue de Lourmel, 75015 Paris, France, Laboratoire de Chimie et Biochimie Pharmacologiques et Toxicologiques (Université Paris Descartes, LCBPT-UMR8601, Paris, F-75006 France; CNRS, LCBPT-UMR8601, Paris, F-75006 France), 45 rue des Saints Péres, 75270 Paris Cedex 6, France, and Institut de Minéralogie et de Physique des Milieux Condensés (Université Pierre et Marie Curie, IMPMC-UMR7590, Paris, F-75005 France; CNRS, IMPMC-UMR7590, Paris, F-75005 France; Université Paris Diderot; IPGP), Campus Boucicaut, 140 rue de Lourmel, 75015 Paris, France

Received May 11, 2007. In Final Form: July 18, 2007

We combine the self-assembly properties of amphiphilic molecules with the radiolysis method to produce specific sizes and shapes of metallic nano-objects. Radiolysis is used to synthesize core−shell structures consisting of nanometric linoleate spherical micelles as the core and silver as the shell. The validity of the technique is asserted by cryoelectron microscopy, which is an adequate technique for low density contrasts and core−shell structures. The shells are found to be homogeneous with a size of a few nanometers. Images are used to bring forward the hypothesis of the fabrication process.

Introduction

Noble metal nanoparticles are now widely present in various fields of research. The interest that they arouse undoubtedly lies in the optical,[1−4] electronic, catalytic, and magnetic properties induced by nanometric dimensions. Since their first successful synthesis[5] in the late 1990s, metallic nanoshells have appeared as a typical system for observing the properties induced by limited size. They are, for example, studied for their ability to enhance optical processes of resonance caused by collective excitations of conduction electrons, and they offer high tunability of their frequency via control of the shell thickness relative to the size of the core.[5−10] They are also used in surface-enhanced Raman scattering[7] (SERS) and critical near-infrared applications such as cancer detection and treatment systems.[11,12] All of these applications require the development of a controlled method that can reliably tailor objects of various dimensions and shapes.

Rapid improvement in the design and fabrication of such nanostructures has been made. Many experimental methods have been implemented to form these shells using chemical[13,14] or physicochemical[8−10,15−17] techniques, and liquid-phase methods have advantages related to their simple application and low cost. So far, they mostly concern the creation of metallic layers on molds consisting of functionalized polystyrene or silica particles with radii ranging from 50 nm to several micrometers in which the metallic layer is initiated with preadsorbed metallic seeds.[13−16]

Because researchers are interested in the physical properties linked to the shells' dimensions, such an approach is necessarily restricted by the difficulties of varying the mold dimensions. Thus, to control the nanostructures' form and size, we propose a flexible solution through the use of self-assembled organic molds as cores to create metallic nanoshells of appropriate dimensions, in particular, of small dimensions.

In this study, we use linoleic acid in an alkaline medium (i.e., an amphiphilic molecule formed by a hydrophobic carbonated chain and a polar carboxylate headgroup). When dissolved in aqueous solution, the acid forms a great variety of structures depending on its concentration and thus offers a large panel of potential templates[18] for synthesizing metal nanostructures. Controlling the mold should then offer a process of highly adjustable morphologies. For our purpose, the size of the elongated tail of the molecule is about 2 nm,[18] which sets the maximum for the micelle radius to this value. We thus look ahead to investigating the sizes of cores well below the usual range.

The fundamental technique in our study is radio-induced reduction through water radiolysis. It consists of irradiating solutions containing metallic ions, with x- or γ-rays that lead to the generation of reducing free radicals. These radicals, in particular, aqueous electrons, provoke the metallic ions to reduce into atoms, and the latter coalesce to form metallic clusters.[19] We applied this radiolysis technique to a solution containing

* Corresponding author.
† Institut des Nanosciences de Paris.
‡ Laboratoire de Chimie et Biochimie Pharmacologiques et Toxicologiques.
§ Institut de Minéralogie et de Physique des Milieux Condensés.

(1) Evanoff, D. D.; Chumanov, G. *J. Phys. Chem. B* **2004**, *108*, 13948.
(2) Mulvaney, P. *Langmuir* **1996**, *12*, 788.
(3) Muskens, O. L.; Del Fatti, N.; Vallée, F.; Huntzinger, J. R.; Billaud, P.; Broyer, M. *Appl. Phys. Lett.* **2006**, *88*, 063109.
(4) Sönnichsen, C.; Franzl, T.; Wilk, T.; von Plessen, G.; Feldmann, J. *New J. Phys.* **2002**, *4*, 93.1.
(5) Oldenburg, S. J.; Averitt, R. D.; Westcott, S. L.; Halas, N. J. *Chem. Phys. Lett.* **1998**, *288*, 243.
(6) Halas, N. In *MRS Bull.* **2005**, *30*, 362.
(7) Jackson, J. B.; Halas, N. J. *Proc. Natl. Acad. Sci. U.S.A.* **2004**, *101*, 17930.
(8) Averitt, R. D.; Sarkar, D.; Halas, N. J. *Phys. Rev. Lett.* **1997**, *78*, 4217.
(9) Jackson, J. B.; Halas, N. J. *J. Phys. Chem. B* **2001**, *105*, 2743.
(10) Sun, Y.; Xia, Y. *Anal. Chem.* **2002**, *74*, 5297.
(11) Hirsch, L. R.; Stafford, R. J.; Bankson, J. A.; Sershen, S. R.; Rivera, B.; Price, R. E.; Hazle, J. D.; Halas, N. J.; West, J. L. *Proc. Natl. Acad. Sci. U.S.A.* **2003**, *100*, 13549.
(12) Hirsch, L. R.; Jackson, J. B.; Lee, A.; Halas, N. J.; West, J. L. *Anal. Chem.* **2003**, *75*, 2377.
(13) Jiang, Z.-J.; Liu, C.-Y. *J. Phys. Chem. B* **2003**, *107*, 12411.
(14) Dong, A. G.; Wang, Y. J.; Tang, Y.; Ren, N.; Yang, W. L.; Gao, Z. *Chem. Commun.* **2002**, 350.
(15) Shi, W.; Sahoo, Y.; Swihart, M. T.; Prasad, P. N. *Langmuir* **2005**, *21*, 1610.
(16) Graf, C.; van Blaaderen, A. *Langmuir* **2002**, *18*, 524.
(17) Pol, V. G.; Grisaru, H.; Gedanken, A. *Langmuir* **2005**, *21*, 3635.
(18) Jönsson, B.; Lindman, B.; Holmberg, K.; Kronberg, B. *Surfactants and Polymers in Aqueous Solution*; John Wiley & Sons: New York, 1998.
(19) Belloni, J.; Mostafavi, M.; Remita, H.; Marignier, J.-L.; Delcourt, M.-O. *New J. Chem.* **1998**, 1239.

10.1021/la701366f CCC: $37.00
Published on Web 08/15/2007 PAGE EST: 3.4

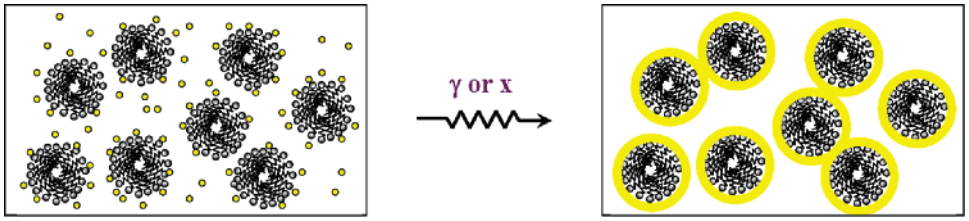

Figure 1. Schematic view of the formation of metallic shells around organic micelles in aqueous solution. The primary silver cations adsorbed at the surface are reduced by the free radicals generated by the γ radiolysis of water and form the metallic layer.

linoleate molecules that were preliminarily self-assembled into spherical micelles. These assemblies, with the polar carboxylate headgroups at the surface, present negative charges that favor the adsorption of silver cations. This was expected to lead to the preferential reduction at the micelle surface which would lead to the formation of silver shells (Figure 1).

The γ-irradiation procedure prefigures a good degree of homogeneity of the formed shells as the energy is absorbed in volume and as the compounds, present in small proportions, are well dispersed. Moreover, fabrication through radiolysis avoids prefunctionalization of the mold or contamination with other compounds by the use of enhancers or seeds. Finally, the absence of seeds should allow the formation of a thin metallic layer on the molds. Previous work has shown the validity of this approach with the silver/fatty acid couple. Indeed, we have succeeded in forming a thickness-controlled silver layer (4 nm) anchored to a behenic acid Langmuir monolayer[20] using grazing incidence angle X-ray irradiation, called surface radiolysis.

Experimental Section

Sample Preparation and γ Irradiation. Silver sulfate (Sigma), absolute ethanol (Prolabo), and linoleic acid (Merck) were pure-grade reagents. Linoleic acid ($CH_3(CH_2)_4CH{=}CHCH_2CH{=}CH(CH_2)_7COOH$) was dissolved in ultrapure water (Millipore system, 18 MΩ cm), and then the pH was adjusted to 11.5 with sodium hydroxide to deprotonate quantitatively the carboxylic groups and form spherical linoleate micelles. Because of the slow spontaneous autoxidation of linoleic acid, only freshly made solutions were used. A concentration of 10 mmol·L^{-1} in linoleate was chosen above its critical micelle concentration, that is, about 2 mmol·L^{-1} at pH ∼11.2.[21,22] Silver sulfate (10 mmol·L^{-1} in Ag^+) was dissolved in the alkaline solution only after the formation of stable linoleate micelles. The concentration of metallic ions was chosen to obtain a significant shell thickness according to their adsorption per section of polar headgroup. This concentration is limited by the formation of AgOH precipitate. Absolute ethanol (0.2 mol·L^{-1}) as $HO^•$ and $H^•$ radical scavengers was added to the solutions. These solutions were then degassed by bubbling with argon prior to irradiation. The solutions were kept away from light at any moment of preparation to prevent the formation of silver nanoparticles by photochemical reduction.

The irradiation experiments were performed with the ^{60}Co source from LCP (Laboratoire de Chimie-Physique) at the Université Paris XI (France) at a dose rate of 4 kGy per hour. During irradiation, solvated electrons and $CH_3C^•HOH$ radicals are formed by the radiolysis of water and act as reducing agents toward silver ions leading to metal atoms. The energy absorbed by the sample, namely, the irradiation dose, was of 20 kGy (20 kJ/kg). This value is, according to the radiolytic yield of reduction of Ag^+ in the presence of linoleate, the dose corresponding to the total reduction of 10 mmol·L^{-1} Ag^+.[23]

Cryoelectron Microscopy Characterization. The samples were observed with transmission electron microscopy in a cryogenic environment known to be adapted to core−shell structures.[24]

The solutions were deposited on 200 mesh holey-carbon-coated grids. After being blotted with filter paper, the grids were frozen by being rapidly plunged into liquid ethane and were mounted and inserted in the microscope using a nitrogen-cooled side entry Gatan 626 cryoholder. Observations were carried out at a temperature of −180 °C in a JEOL 2100F electron microscope equipped with a URP objective lens (Cs, 0.5 mm; Cc, 1.1 mm; focal length, 1.9 mm) using an accelerating voltage of 200 kV with the following illumination conditions: alpha 3, spot 4, 100 μm condenser aperture, and 50 μm objective aperture. Images were recorded using the MDS minimum electron dose system (10 electrons per $Å^2$) at a magnification of 60 000× on Kodak So163 film. For each field, images were recorded using a different defocus value further from focus for good visualization of the particles.

By freezing the system as is, cryoelectron microscopy ensures the observation of soft nano-objects in equilibrium in solution because it avoids the phase transition and possible particle aggregation resulting from drying procedures.

To ensure good image analysis, we corrected the contrast transfer function (CTF) of the electron microscope as follows. According to the strategy proposed in ref 25, we first rejected the cryoelectron micrographs whose enhanced power spectrum density (PSD) images did not show visible diffraction rings or contained drifting diffraction rings. We estimated the parameters of the CTF for each of the remaining images using the CTF estimation algorithm of the Xmipp image processing package.[26] This algorithm estimates the CTF parameters by simultaneously minimizing the distance of the fitted theoretical PSD model from the experimental PSD and the correlation between the enhanced experimental PSD and the corresponding theoretical model.[27,28] The CTF was then corrected on each experimental image in the SPIDER image processing package[29] by applying the Wiener filter computed for the corresponding CTF parameters.[30]

Results and Discussion

A sample that had not been submitted to ionizing rays was first observed to verify that no metallic coverage was initiated previously to irradiation. The micelles that have been observed (Figure 2) have a measured radius of about 1.6 nm. This is slightly smaller than the expected 2 nm length of linoleate molecules, suggesting that the tails are not totally elongated.

Cryo-TEM observation of the irradiated samples is shown in Figure 3; it reveals larger objects that are quite homogeneously

(20) Muller, F.; Fontaine, P.; Rémita, S.; Faure, M.-C.; Lacaze, E.; Goldmann, M. *Langmuir* **2004**, *20*, 4791.
(21) Gebicki, J. M.; Allen, A. O. *Phys. Chem.* **1969**, *73*, 2443.
(22) Hauville, C.; Rémita, S.; Thérond, P.; Rouscilles, A.; Couturier, M.; Jore, D.; Gardès-Albert, M. *Radiat. Res.* **1998**, *150*, 600−8.
(23) Rémita, S.; Fontaine, P.; Rochas, C.; Muller, F.; Goldmann, M. *Eur. Phys. J. D* **2005**, *34*, 231.
(24) Crassous, J. J.; Ballauff, M.; Drechsler, M.; Schmidt, J.; Talmon, Y. *Langmuir* **2006**, *22*, 2404.
(25) Jonic, S.; Sorzano, C. O.; Cottevieille, M.; Larquet, E.; Boisset, N. *J. Struct. Biol.* **2007**, *157*, 156−67.
(26) Sorzano, C. O.; Marabini, R.; Velazquez-Muriel, J.; Bilbao-Castro, J. R.; Scheres, S. H.; Carazo, J. M.; Pascual-Montano, A. *J. Struct. Biol.* **2004**, *148*, 194−204.
(27) Sorzano, C. O.; Jonic, S.; Nuñez, R.; Boisset, N.; Carazo, J. M. *J. Struct. Biol.*, submitted for publication.
(28) Velazquez-Muriel, J. A.; Sorzano, C. O.; Fernandez, J. J.; Carazo, J. M. *Ultramicroscopy* **2003**, *96*, 17−25.
(29) Frank, J.; Radermacher, M.; Penczek, P.; Zhu, J.; Li, Y.; Ladjadj, M.; Leith, A. *J. Struct. Biol.* **1996**, *116*, 190−9.
(30) Franck, J.; Penczek, P. A. *Optik* **1995**, *98*, 125−129.

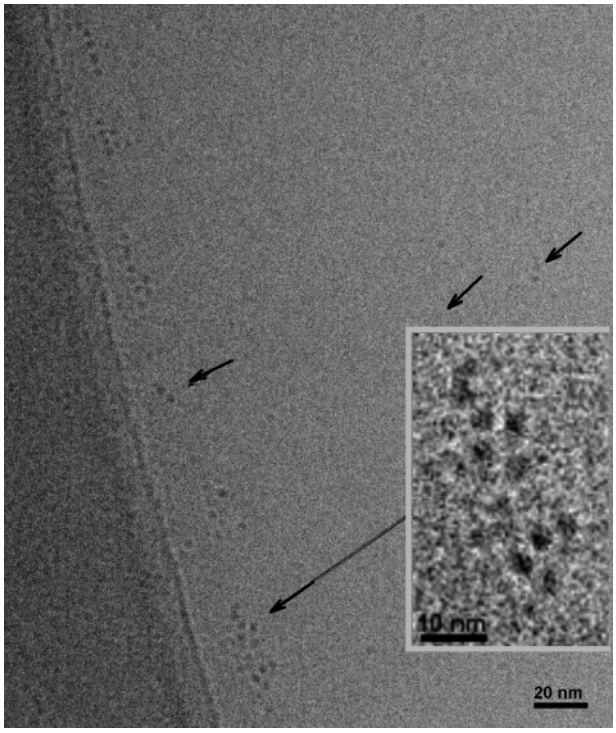

Figure 2. Cryo-TEM image (at a defocus of about −2.1 μm) of an aqueous sample of linoleate (3 mmol·L^{-1}) and silver ions (10 mmol·L^{-1}) that has not been irradiated. It exhibits spherical low-density objects with a mean radius of 1.6 nm attributed to organic micelles. The inset shows enhanced contrast for diameter measurements.

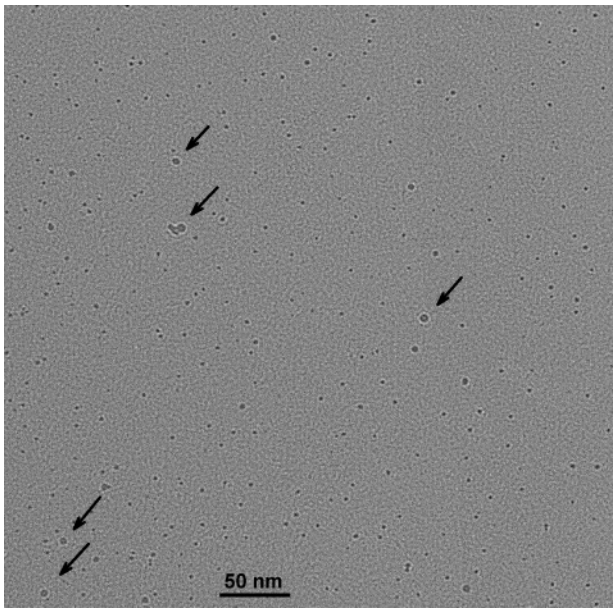

Figure 3. Cryo-TEM image (at a defocus of about −1.8 μm) of an aqueous sample of linoleate (10 mmol·L^{-1}) and silver ions (10 mmol·L^{-1}) that has been irradiated with γ-rays up to 20 kGy. It exhibits spherical high-density objects that are well dispersed on the grid with a little disparity in size.

dispersed on the grid, with little aggregation. Figure 4a−d shows details of the larger objects (indicated by arrows). These appear to be shells: the density loss at the center of these high-density objects indeed indicates that they correspond to metallic structures with a core made out of low-density material that we attribute to the organic phase.

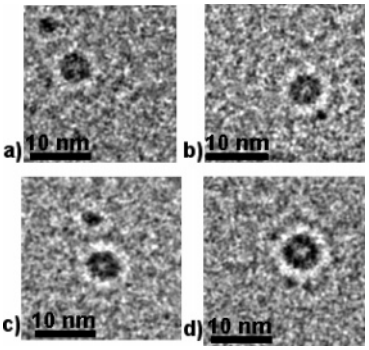

Figure 4. Cryo-TEM images (at a defocus of about −1.8 μm) of an aqueous sample of linoleate (10 mmol·L^{-1}) and silver ions (10 mmol·L^{-1}) that has been irradiated with γ-rays up to 20 kGy. The enlarged zones from Figure 3 exhibit spherical high-density objects presenting a density loss at the center attributed to the core−shell structures. They display, respectively, external and core radii of (a) 2.4−0.9 nm, (b) 2.5−1.0 nm, (c) 2.5−0.9 nm, and (d) 2.9−1.0 nm, which lead to mean values collected over the image of 2.6−0.9 nm. Figure 4a,c exhibits spheres (small objects) of high density with no density loss and smaller size. They are attributed to isolated silver aggregates in the bulk. Displayed diameters over the image shown in Figure 3 range from 1.0 to 2.8 nm.

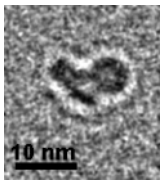

Figure 5. Cryo-TEM image (at a defocus of about −1.8 μm) of an aqueous sample of linoleate (10 mmol·L^{-1}) and silver ions (10 mmol·L^{-1}) irradiated with γ-rays up to 20 kGy. The enlarged zone from Figure 3 displays a pin-shaped object with a shell.

The formed silver layer seems to be unbroken and rather homogeneous for most of the core−shell structures. The nanoshell dimensions appear to be quite homogeneous in terms of core size and shell thickness. Within the inherent limits of microscopy, the numeric treatment allows us to measure an external diameter of 2.6 nm. Nevertheless, the internal, or core, radius is estimated from saturation through the outer shell so that we shall state that its value is greater than 0.9 nm.

Two possibilities emerge for this measured core value. On the one hand, an actual core radius of 0.9 nm indicates a diminution of micelle size, from 1.6 nm prior to irradiation. This phenomenon could be attributed to silver metallization that may constrain the carbonic chains' extension. In this case, the shell thickness is about 1.7 nm. On the other hand, if the radii discrepancy is due to the saturation of electron beam absorption, taken to the extreme, then it means that the actual core is as large as in Figure 2 but is "hidden" by contrast limits. Then, the silver shell thickness is 1.0 nm. The aspect ratio of the core radius on the external radius then ranges from 0.35 to 0.61. To our knowledge, these are the smallest metallic nanoshells ever observed. The shells of Figure 3 and 4 are the most frequent core−shell structures observed. However, structures such as the ones in Figure 5 can also be observed. Figure 5 shows an object composed of a shell and a pin-shaped part. This one is most likely an "opened" shell or a metallic layer over an asymmetric linoleate self-assembly, which is more evidence that the apparent density loss is not an artifact but represents an actual morphology characteristic.

In addition to these nanoshells, the cryo-TEM observations evidenced other, mainly spherical, objects in the solution (small objects in the upper part of Figure 4a,c) showing that the process

does not prevent the formation of spherical clusters. All of the small, high-density objects displayed in Figure 3 are spheres and have diameters of up to 2.8 nm. The formation of such isolated spheres can be explained by the competitive mechanism between reduction in the bulk and reduction onto the micelles. The proportion of preadsorbed ions on the micelle surface and the diffusion kinetics of silver ions to the surface during the synthesis, which have not yet been totally controlled, are the two parameters that are bound to facilitate one mechanism or the other. The presence of germs in the bulk solution, prior to irradiation, may also provoke the aggregation of reduced atoms far from any micelle during the irradiation step.

Conclusions

We succeeded in extending the surface radiolysis procedure to a 3D process with respect to forming organometallic nanoshells. For this purpose, we combined the self-assemblies properties to obtain an organic spherical core and the radiolysis technique to form a metallic shell. Such a procedure allowed us to obtain objects of nanometric dimensions that are smaller than the equivalent structures that have been presented in the literature.

The formation process of these nanoshells is not entirely understood, especially the mechanism of shell growth because two hypotheses are likely to explain the observable result: layer-by-layer growth or growth induced by germs of atoms on the micelle surface and expansion over all of the micelle with the resulting thickness. As initiated in the present experiments, we aim to maneuver concentrations, irradiation doses, and dose rates to control the size of the formed nanostructures. To follow the intermediate steps in nanoshell formation, a series of samples shall be used to study the effects of silver ion concentration and irradiation dose. Because the thickness of the metallic layer depends on these parameters, there is indeed the possibility of adjusting the aspect ratio. Varying the dose rate shall allow us to exploit the homogeneity of the metallic layer. Eventually, full control of the parameters shall allow us to favor the relative concentration of the desired objects and segregate them with respect to the optical properties (plasmon absorption) as a function of the aspect ratio of the shells.

The variety of self-assembled structures formed by the amphiphilic molecules also offers a large panel of molds leading to various nanometric organometallic devices.

Acknowledgment. We thank Dr. Hynd Remita from LCP Orsay for access to the γ source.

LA701366F